Published in final edited form as:
Neuroscience. 2010 February 17; 165(4): 1501. doi:10.1016/j.neuroscience.2009.11.004.

HETEROGENEOUS DOPAMINE POPULATIONS PROJECT TO SPECIFIC SUBREGIONS OF THE PRIMATE AMYGDALA

Y. T. CHO[a] and **J. L. FUDGE**[a,b,*]

[a]Department of Neurobiology and Anatomy, University of Rochester School of Medicine and Dentistry, 601 Elmwood Avenue, Rochester, NY 14642, USA

[b]Department of Psychiatry, University of Rochester School of Medicine and Dentistry, 601 Elmwood Avenue, Rochester, NY 14642, USA

Abstract

Amygdala dysfunction has been reported among patients with various psychiatric disorders, and dopamine is critical to the amygdala's ability to mediate fear conditioning. Recent work indicates that the midbrain dopaminergic neurons have heterogeneous receptor and membrane channel profiles, as well as differential physiologic responses to discrete stimuli. To begin understanding how dopamine affects amygdala physiology and pathology in higher primates, we mapped the inputs from the midbrain dopaminergic neurons to various amygdala nuclei in the monkey using retrograde and anterograde tracing techniques, and single and double immunofluorescence histochemistry for tracer and tyrosine hydroxylase, a dopamine marker. Our results show that the primate amygdala as a whole receives broad input, mostly from the dorsal tier of the substantia nigra, pars compacta, and the A8-retrorubral field. Input from the A10-ventral tegmental area, while present, was less prominent. These results differ from data in the rat, where the midline A10-ventral tegmental area is a major source of dopamine to the amygdala "mesolimbic" pathway. Both the "amygdala proper" and the "extended amygdala" receive the majority of their input from the dorsal tier of the substantia nigra and A8-retrorubral field, but the extended amygdala receives additional modest input from the ventral tier. In addition, the "extended amygdala" structures have a denser input than the "amygdala proper," with the exception of the lateral core of the central nucleus, which receives no input. Our anterograde studies confirm these findings, and revealed fine, diffuse terminal fibers in the amygdala proper, but a denser network of fibers in the extended amygdala outside the lateral core of the central nucleus. These results indicate that the entire extent of the dorsal tier beyond the A10-ventral tegmental area may regulate the amygdala in primates, and subsequently serve as a source of dysfunction in primate psychopathology.

Keywords

extended amygdala; ventral tegmental area; retrorubral field; dorsal tier; ventral tier; substantia nigra

The limbic system is a distributed neural network of cortical and subcortical structures that coordinate emotional awareness and responses to the environment. The amygdala, a heterogeneous limbic structure residing in the medial temporal lobe, assigns emotional salience to events and coordinates with other limbic regions, including the pre-frontal cortex (PFC) and the hippocampus. Recent studies in animal models and humans indicate that functional

*Corresponding author. Tel: +1-585-273-2028; fax: +1-585-756-5334. julie_fudge@urmc.rochester.edu (J. L. Fudge)..

abnormalities of the amygdala, and the limbic system as a whole, contribute to the pathophysiology of depression, as well as other psychiatric illnesses (Phillips et al., 2003a,b).

A major function of the amygdala is fear conditioning, as confirmed in animal and human studies (Phillips and LeDoux, 1992; Pitkanen et al., 1997; Alvarez et al., 2008). Fear conditioning facilitates rapid protective responses to negative stimuli, representing a key survival method for animals and humans. Yet hypersensitivity to fear conditioning may lead to misinterpretation of external stimuli as emotionally relevant or inappropriately negative. This may lead to negative thought patterns, anxiety, and ruminative thinking, all common symptoms of depressive illnesses (Wenzlaff et al., 1988; Oaksford and Stenning, 1992). Over-active amygdalar functioning has been demonstrated among patients with depression, suggesting that hyperactivity in this area correlates with depressive illnesses (Sheline et al., 2001; Siegle et al., 2002).

Dopamine (DA) is a key neurotransmitter involved in fear conditioning, and the amygdala's ability to acquire and express fear conditioning strongly depends on intact dopamine pathways. The DA neurons are now recognized as a heterogeneous cell group, and the A10-ventral tegmental area (A10-VTA) is the main source of DA to the amygdala based on studies in rodents (review; Bjorklund and Dunnett, 2007). In rats, disruption of the A10-VTA, with subsequent decreased DA release to the amygdala, impairs retrieval of previously learned fear conditioning (Nader and LeDoux, 1999). Similarly, infusion of either D1 or D2 receptor antagonists into the amygdala of rats leads to impaired acquisition, consolidation and retrieval of learned fear conditioning (Guarraci et al., 1999, 2000; Greba and Kokkinidis, 2000; Greba et al., 2001; Fadok et al., 2009). These studies suggest that DA is necessary for different facets of fear conditioning, including the learning process of pairing an unconditional stimulus (shock) to a conditional stimulus (sound), the storage process needed to use this information for future experiences, and the ability to recall this information when necessary. Confirming the importance of DA in fear conditioning in humans, a combined positron emission tomography (PET)-ligand and functional magnetic resonance imaging (fMRI) study showed that amygdala activation in response to aversive stimuli correlated with an increase in amygdalar dopamine storage capacity (Kienast et al., 2008). The latter study points to the importance of understanding DA innervation of the amygdala in higher species.

Current knowledge of the mesolimbic projection rests on lesion and double-labeled tracer studies in rat. Tracer studies in the non-human primate have mapped midbrain inputs to the amygdala as part of larger studies examining subcortical and/or cortical afferents, but none of these studies confirmed the dopaminergic status of these inputs (Aggleton et al., 1980; Mehler, 1980; Norita and Kawamura, 1980). In addition, the heterogeneous composition and function of the amygdala nuclei lends itself to anatomic studies aimed at understanding the specific subregions of the amygdala. Therefore, our study's goal was to map the DAergic inputs to specific nuclei of the primate amygdala, with an analysis of the specific DA subpopulations involved.

EXPERIMENTAL PROCEDURES

Primate injections and surgeries

Eleven *Macaca fascicularis* monkeys, weighing between 3 and 9 kg, were used in these experiments (Labs of Virginia, Yemassee, SC, USA; Three Springs Laboratories, Pekaski, PA, USA, and Worldwide Primates, Tallahassee, FL, USATracers). Small amounts (40 nl) of either Lucifer Yellow conjugated to dextran amine (LY; 10% Molecular Probes, Eugene, OR, USA), Fluoro-Ruby conjugated to dextran amine (FR; 4% Molecular Probes) or Fluorescein conjugated to dextran amine (FS; 10% Molecular Probes) were injected into the central nucleus, amygdalostriatal area, interstitial nucleus of the posterior limbic of the anterior commissure

(IPAC), medial nucleus, accessory basal (magnocellular and parvicellular subdivisions) and basal (magnocellular and parvicellular subdivisions) nuclei of the amygdala. To confirm retrograde studies, we placed bidirectional tracers at several mediolateral and rostrocaudal levels of the midbrain DA neurons to determine the pattern of anterogradely labeled fibers in the amygdala.

All experiments were carried out according to National Institutes of Health guidelines, and reviewed by the University of Rochester Committee on Animal Research. Animals were given i.m. injections of ketamine hydrochloride (10 mg/kg) (Hospira, Inc., Lake Forest, IL, USA), intubated, and deeply anesthetized with i.v. pentobarbital (initial dose 20 mg/kg), which was maintained as needed during surgery. We performed a craniotomy to visualize cortical surface landmarks, and electrophysiologic mapping to locate internal landmarks such as the anterior commissure, striatum and amygdala (Fudge et al., 2004; Fudge and Tucker, 2009). Stereotaxic coordinates for these boundaries were determined, and the locations of the nuclei were estimated. The retrograde tracer was pressure-injected over 10–15 min into individual nuclei using a 0.5 μl Hamilton syringe (Hamilton Company, Reno, NV, USA), and the syringe was left in place for 20 min to prevent leakage of tracer up the syringe track. Only one injection of each tracer was used per animal. After injections were placed, the bone flap was replaced and the overlying musculature and skin sutured. Prophylactic antibiotics and pain medication were given for 7–10 days post-operatively.

Ten to thirteen days after surgery, animals were deeply anesthetized and killed by perfusion through the heart with 0.9% saline containing 0.5 ml of heparin sulfate (200 ml/min for 10 min), followed by cold 4% paraformaldehyde in 0.1 M phosphate buffer/ 30% sucrose solution (100 ml/min for 1 h). The brain was removed, placed in fixative overnight, and sunk in increasing gradients of sucrose (10%, 20%, 30%). Brains were cut on a freezing microtome (50 μm sections) and saved in cryoprotectant solution (30% ethylene glycol and 30% sucrose in 0.1 M phosphate buffer) at −20 °C (Rosene et al., 1986). Every 24th slice was used in our studies, and adjacent sections were used for determining anatomical landmarks.

Single-labeling immunocytochemistry

Tracers—Sections were thoroughly rinsed in 0.1 M phosphate buffer (pH 7.2) with 0.3% Triton-X (PB-TX). After treatment with endogenous peroxidase inhibitor for 5 min, followed by more rinses, sections were pre-incubated in a blocking solution of 10% normal goat serum in 0.1 M PB-TX (NGS-PB-TX) for 30 min. Tissue was then placed in primary antisera to LY (1:2000, Molecular Probes, rabbit), FS (1:2000, Molecular Probes, rabbit), or FR (1:1000, Molecular Probes, rabbit) for approximately 96 h at 4 °C. After thorough rinsing with 0.1 M PB-TX, and pre-incubation with 10% NGS-PB-TX, sections were incubated in biotinylated secondary anti-rabbit antibody. Tracers were visualized using the avidinbiotin reaction (Vector ABC Standard kit, Burlingame, CA, USA). Additional compartments for each case were also processed for tracer enhanced with nickel intensification (3, 3′-diaminobenzidine tetrahydrochloride with 1% nickel ammonium sulfate and 1% cobalt chloride, catalyzed by 0.03% hydrogen peroxide for 1–2 min) and counterstained with acetylcholinesterase (AChE) (Geneser-Jensen and Blackstad, 1971) or cresyl violet.

Calbindin-D28k (CaBP)—Adjacent or near adjacent sections through the ventral midbrain were used to demarcate the dorsal and ventral tiers of the SNpc according to CABP immunoreactivity (Lavoie and Parent, 1991; German et al., 1992). Sections were thoroughly rinsed, and preincubated in 10% NGS-PB-TX as described above, and then incubated for 96 h in CaBP (Chemicon, 1:10,000, mouse) antisera. Sections were then rinsed, blocked and incubated in secondary anti-mouse biotinylated antibody. Following thorough rinsing, CaBP protein was visualized using the avidin–biotin reaction described above.

Double-labeling fluorescent immunocytochemistry

Optimal dilutions for primary antibodies used in immunofluorescent studies were established in advance using single-label fluorescent labeling. In addition, control tissue from animals without tracer injections and immunohistochemical processing was examined for autofluorescence. The primary antibodies used were (1) tyrosine hydroxylase (TH; mouse, Millipore, Temecula, CA, USA) diluted to 1:5000, and antiserum to one of the following: (2) Lucifer Yellow tracer (LY; rabbit, Molecular Probes, Eugene, OR, USA) diluted to 1:3000; Fluorescein (FS; rabbit, Molecular Probes) diluted to 1:750; or Fluoro-Ruby (FR; rabbit, Molecular Probes) diluted to 1:2000. Fluorescent immunocytochemistry was run on coronal sections from the level of the mammillary bodies rostrally to the emergence of the brainstem A5 catecholamine group caudally. For each injection site, every twenty-fourth slice was pulled from storage in a −20 °C freezer and rinsed for 15 min in four successions in 0.1 M phosphate buffer with 0.3% Triton-X100 detergent (PB-TX) (pH=7.2), and then overnight in PB-TX (pH=7.2) in a 4 °C cold room. The following day, the tissue was rinsed for 5 min in a solution of: 80% 0.1 M phosphate buffer (PB) (pH=7.2), 10% methanol, and 3% hydrogen peroxide solution. The tissue was rinsed for six successions of 15 min in 0.1 M PB-TX (pH=7.2), blocked for 30 min in 10% normal goat serum (NGS) made in 0.1 M PB-TX (pH=7.2), and then incubated for four nights with two primary antibodies—TH and tracer—in a solution of 10% NGS.

After four nights, the tissue was rinsed for 15 min in six successions in 0.1 M PB-TX (pH=7.2), then blocked for 30 min in 10% NGS. The tissue then incubated at room temperature in the dark with pooled secondary antibodies for 4 h in a solution of 10% NGS (pH=7.2). Following preliminary experiments to determine that labeling from the two fluorophors was similar for each antigen, the secondary antibodies used were (1) AlexaFluor 488 nm, goat anti-mouse (against TH) at a concentration of 50 μl/10 ml of 10% NGS, plus either: (2) AlexaFluor 546 nm, goat anti-rabbit (against tracer) at a concentration of 50 microliters/10 ml of 10% normal goat serum; or Texas Red 596 nm (Genway Biotech, Inc., San Diego, CA, USA), goat anti-rabbit (against tracer, at a dilution of 1:500 in 10% NGS). After 4 h, tissue was rinsed for six successions of 15 min in 0.1 M PB (pH=7.2). Tissue was mounted on gelatin-subbed slides out of 0.1 M PB (pH=7.2), dried overnight, and coverslipped with Vectashield medium (Vector Lab, Burlingame, CA, USA). Mounted and coverslipped slides were stored in the dark at 4 ° C until taken to the microscope for viewing.

Analysis

Neurolucida drawings for retrograde studies—Slides containing retrograde-labeled cells were viewed and charted on an Olympus Ax70 Fluorescent Microscope equipped with cubes for viewing 488 and 546 or 596 nm wavelength antibodies. Using a video CCD camera attached to the microscope and interfaced with the computer, cells and major anatomical landmarks were drawn using the computer program, Neurolucida (MicroBrightfield Inc., Rutland, VT, USA), under 10× objective. To visualize cells in both the green and red channels, we used an exposure of 1.47 s, with a gain of 1.58. Tracer-labeled cells were charted first, and the cube was then switched to view TH-positive cells. Double labeled cells were marked based on identical position and morphology between tracer-labeled and TH-labeled cells. These drawings were transferred to Adobe Illustrator for formatting.

Identifying the dorsal and ventral tier—Adjacent or near-adjacent sections through the ventral midbrain stained with Nissl or for CABP immunoreactivity were used to identify the dorsal and ventral tier subpopulations. For those slides stained for CABPimmunoreactivity, images were projected onto a wall using a macroprojector (JENA, Germany), and the boundaries between the dorsal and ventral tiers, and the substantia nigra, pars reticulate (SNpr), were drawn by hand onto hard copies of the Neurolucida charts. The projected image was

aligned with the Neurolucida drawing using major landmarks such as the cerebral peduncles, aqueduct, and blood vessels. For slides stained with Cresyl Violet, we used camera lucida techniques to project and align images onto Neurolucida paper charts. Dorsal tier and ventral tier were distinguished by soma size and dendrite orientation.

Confocal microscopy—To confirm information obtained with traditional fluorescent microscopy, and better visualize the morphology of double-labeled neurons, we examined some cases using confocal microscopy. A FV1000 Olympus confocal with SIM scanner was used with Alexa Fluor 488 nm (green) and Texas Red 596 nm (red) configurations. The area of interest was first identified using a 4× objective with widened pinhole. Once double-labeled cells were seen, they were examined with oil immersion under 20× and 40× power. The objective was focused at the top and bottom of the z-plane through the cell and the area was scanned every 0.8 μm, making a stack of 14–15 slices. A Kalman setting of 6 was used for the best resolution.

Anterograde studies—We examined the distribution of labeled fibers in the amygdala using dark-field microscopy with a 10× and 20× objective. Hand-drawn charts were created using camera lucida techniques and then scanned into the computer. The distribution of labeled fibers within specific amygdala subdivisions was determined using adjacent Nissl and CABP-immunoreactive sections, which were carefully aligned with charts to match anatomic landmarks such as blood vessels (Pitkanen and Amaral, 1993).

RESULTS

Amygdaloid nuclei

We describe the primate amygdaloid nuclei outside of the CeN according to Price, Amaral and colleagues (Price et al., 1987; Amaral et al., 1992). The lateral nucleus borders the external capsule. The medially adjacent basal nucleus is subdivided into magnocellular (Bmc), intermediate (Bi) and parvicellular subdivisions (Bpc) (Fig. 1). AChE activity is highest in the magnocellular subdivision and declines along a gradient in the intermediate and parvicellular subdivisions of the basal nucleus (Amaral and Bassett, 1989). The paralaminar nucleus (PL) forms a thin sheet surrounding the basal nucleus rostrally and caudally, and the intercalated cell islands are interposed between major nuclei. The latter two subregions are seen best in Nissl stained sections. The accessory basal nucleus is composed of magnocellular (ABmc), parvicellular (ABpc), and “sulcal” (ABs) subdivisions. The magnocellular and sulcal subdivisions have relatively higher AChE staining compared to the parvicellular subdivision. The sulcal subdivision of the accessory basal nucleus is caudomedially adjacent to the amygdalohippocampal area (also high in AChE). Its inclusion in the amygdalohippocampal area (AHA) has been suggested based on some neurochemical and connectional similarities (Amaral and Bassett, 1989; Pitkanen and Amaral, 1998). Along the medial aspect of the amygdala are the anterior and posterior cortical nuclei (CoA and CoP, respectively), the medial nucleus (M), and the periamygdaloid cortex (PAC). The periamygdaloid cortex is divided into four zones with varying degrees of differentiation (PAC I-III and PACs). The sulcal subdivision (PACs) is located around the amygdaloid fissure (semiannular sulcus), and is the least differentiated.

The CeN subdivisions are described using the nomenclature of deOlmos (DeOlmos, 1990) and Martin (Martin et al., 1991) in primates. The CeN and its lateral transition regions with the striatum—the amygdalostriatal area and IPAC—are considered part of the “central extended amygdala” (Alheid, 2003). In monkey, the medial subdivision of the CeN (CeM) contains moderate AChE activity and sweeps dorsomedially around the CeLcn and into the basal forebrain. In contrast, the CeLcn, or lateral central core subdivision, an oval structure

encapsulated by fibers of the stria terminalis, contains very low AChE activity (DeOlmos, 1990; Sakamoto et al., 1999; Freedman and Shi, 2001; Fudge and Haber, 2002). The amygdalostriatal area and IPAC are both subdivided into medial and lateral areas, based on cellular and histochemical features (Fudge and Tucker, 2009). The IPAC merges caudally with the amygdalostriatal area and forms a ventromedial transition zone with the caudoventral putamen.

Placement of injection sites

Amygdala injection sites—A total of 17 injection sites were previously placed within discrete nuclei (Fig. 2a–c). Nine injection sites were analyzed in the amygdala proper. Within the basal nucleus, we analyzed two injections in the magnocellular division (Bmc: J8FR, J12FR) and three in the parvicellular division (Bpc: J14FR, J15FS, J20LY) (Table 1, Fig. 2). J15FS was placed in the caudal Bpc and straddles the paralaminar nucleus, while J14FR straddles the paralaminar nucleus more rostrally. In the accessory basal nucleus we analyzed two cases with injections in the magnocellular division (ABmc: J8LY, J12FS) and two with injections in the parvicellular division (ABpc: J18FR, J20FS). J20FS encroaches slightly into the ABmc.

Eight injections sites were placed within the extended amygdala. Two injections were confined to the medial nucleus (MeN: J16FR, J19LY). Within the central nucleus, two injection sites were confined to the lateral core subdivision (CeLcn: J1LY, J9FS), and one to the medial subdivision (CeM: J9LY). Two cases had injections located in the IPAC (IPAC: J7FR and J7FS). One injection was placed in the amygdalostriatal area, in both its medial and lateral components (Astr: J9FR). Although there continues to be some debate as to whether the IPAC and amygdalostriatal area are part of the extended amygdala, or are part of the striatum (Zahm et al., 1999; Alheid, 2003), we grouped these areas as part of the extended amygdala, with the hypothesis that their pattern of innervation from the DAergic midbrain would be similar to the "extended amygdala" rather than to the cortical-like "amygdala proper." The Bi, the lateral nucleus, much of the "cortical amygdala" (periamgydaloid cortex, CoA and CoP) and the bed nucleus of the stria terminalis (BNST) were not injected in this set of experiments.

Ventral midbrain injections—Five injections of a bidirectional tracer were placed at various levels within the ventral midbrain and analyzed for anterogradely labeled fibers in order to confirm general observations of our retrograde results (Table 1, Fig. 2d–f). At the rostrocentral level, J15FR was confined to the medial A9-dt, with little encroachment into the ventral tier. J21FS was centered mediolaterally on the A9-SNpc and spanned the dorsal and ventral tiers. J20FR was injected only into the A9-vt. Within the caudal half of the midbrain, two injections were placed in the A8-retrorubral field (A8-RRF), J16FS and J19FS, with J16FS being caudal and medial to that of J19FS.

Subpopulations of the midbrain DA neurons

To define the boundaries of the classic A8-A9-A10 DAergic groups, we used landmarks previously described by Hirsch et al., and used in human and monkey studies (Hirsch et al., 1988; Francois et al., 1999) (Fig. 3). This methodologic scheme standardizes the boundaries of the DA cell groups (Fuxe et al., 1970) and the concept of the dorsal and ventral tier (Lavoie and Parent, 1991). The rostral boundary of the midbrain DAergic groups was defined by the mammillary bodies, and the caudal boundary was the emergence of the pedunculopontine nucleus. For the A10-VTA at more rostral levels, the lateral boundary was defined as the vertical edge bisecting the red nucleus, and the medial edge was the midline. The A9 group as a whole was bound medially by the lateral edge of the A10-VTA group, dorsolaterally by the medial lemniscus, and ventro-laterally by the SNpr. The A9-substantia nigra pars compacta refers to both dorsal and ventral tier components (A9-dt and A9-vt), with A9-dt defined by its

calbindin-positive soma, and A9-vt by its calbindin-negative immunoreactivity (Fig. 4) (Lavoie and Parent, 1991). The SNpr was marked by thick calbindin-positive fibers ventral to the A9-vt. The A8-RRF group emerged in the caudal half of the ventral midbrain, and, along with A10-VTA and A9-dt, was considered part of the dorsal tier based on CaBP-immunoreactivty. A8-RRF was bound medially by the lateral edge of cranial nerve III, and included all cells located within or dorsomedial to the medial lemniscus. Cells located lateral to the medial lemniscus were caudal extensions of the A9 group. Caudally, the lateral edge of cranial nerve III formed the lateral boundary of the A10-VTA group.

Double immunofluorescent studies

The pattern of double-labeled cells across different cases was similar among specific nuclear regions, with the exception of the Bpc, where an injection into the caudal pole resulted in a unique distribution of double-labeled cells. A representative case for each amygdala subregion is described below in detail, with additional information for the Bpc. The pattern of TH/tracer labeled cells from each case was compared to sections single-labeled for tracer only using DAB staining. In all cases, the distribution of single-labeled (DAB processed) and double-labeled (immunofluorescence) cells was similar.

Amygdala proper

Basal, magnocellular (Bmc)—A moderate number of double-labeled cells resulted from injections placed within the Bmc (Fig. 5, Table 2). A few double-labeled cells were located in the rostral portion of the ventral midbrain, mostly in A9-dt. Midway through the ventral midbrain, a moderate number of double-labeled cells began to emerge, and these spread mostly along the medio-lateral expanse of the A9-dorsal tier, and the lateral A10-VTA. As A8-RRF began to emerge, a significant number of FR/TH-positive cells were found in this area, and continued to be present as this area widened caudally. The caudal extension of A9-dt, as well as the caudal lateral A10-VTA, also continued to contain double-labeled cells. The caudal-most extension of A8-RRF contained few to no double-labeled cells.

Basal, parvicellular (Bpc)—Far fewer double-labeled cells resulted from injections into this subregion of the basal nucleus, compared to the Bmc (Fig. 6). For two of the three cases (J14FR, J20LY), double-labeled cells were not found until the A8-RRF began to emerge. Double-labeled cells were then located mostly in the A8-RRF, with a few cells in the lateral A10-VTA. Few to no double-labeled cells were found in the caudal-most extension of A8-RRF or the A9-SNpc. In contrast to cases J14FR and J20LY, the injection site in J15FS was placed in the caudal pole of the Bpc. There were far more double-labeled cells resulting from this injection. Double-labeled cells were found mid-way through the midbrain, and were located in the lateral A10-VTA and lateral A9-SNpc, both in the A9-dt, as well as a few in the A9-vt. As the A8-RRF began, a moderate number of double-labeled cells were found in this group, as well as the caudal extension of the A9-dt.

Accessory basal, magnocellular (ABmc)—A moderate number of double-labeled cells were found following injections into the ABmc. In these cases, double-labeled cells spanned the medio-lateral extent of the A9-dt. In general, the medial A9 group contained a moderate density of double-labeled cells, which continued into the lateral A10-VTA group. The A8-RRF also contained a moderate number of double-labeled cells, though the caudal-most extension of the A8-RRF contained few to no double-labeled cells. In contrast to other cases with injections in the amygdala proper, a modest number of double-labeled cells were also found in A9-vt.

Accessory basal, parvicellular (ABpc)—Overall, far fewer double-labeled cells resulted from injections into the ABpc, compared to injections into the ABmc. A few double-labeled

cells were located in the A10-VTA and A9-dt, with slightly more double-labeled cells located in the A8-RRF. The injection site for J20FS appeared to encroach slightly into the ABmc, however, the pattern of double-labeled cells resembled that of case J18FR, which was confined to the ABpc, suggesting that little tracer was taken up by terminals in the ABmc.

Extended amygdala

Medial nucleus (MeN)—The medial nucleus is considered part of the "medial extended amygdala," and is distinct from structures of the "central extended amygdala." More double-labeled cells were found following injections placed in the MeN compared to those placed in the amygdala proper (Figs. 7 and 8). In general, there were few to no double-labeled cells in the rostral midbrain. Mid-way through the midbrain, a substantial proportion of double-labeled cells were found in the A9-dt, with a few in the A10-VTA. More caudally, most of the double-labeled cells were found within the boundaries of A8-RRF, with a few in the A10-VTA. (Table 2).

Central nucleus, medial division (CeM)—A large number of cells were double-labeled in this case (Fig. 9). Double-labeled cells began to emerge mid-way through the ventral midbrain, and were located mostly in the A9-dt throughout its entire medio-lateral expanse. A moderate number of double-labeled cells were also found in the A9-vt. A moderate amount of double-labeled cells were found in the A10-VTA, a trend that continued caudally. A substantial number of double-labeled cells were found in the A8-RRF, and a few were found in the caudal extensions of the A9-dt and A9-vt, as well. Few to no double-labeled cells were found in the caudal-most extension of the A8-RRF.

Central nucleus, lateral core subdivision (CeLcn)—Few to no single-labeled cells were found in the entire ventral midbrain, following two injections confined to the CeLcn. Because no single-labeled cells were found on DAB ICC, these cases were not run for double immunofluorescent staining.

Amygdalostriatal area—A large number of double-labeled cells were found throughout the ventral midbrain. Mid-way through the midbrain, double-labeled cells were located mostly in the A9-dt, and followed the entire mediolateral expanse of the A9-dt. Similar to the CeM (J9LY), double-labeled cells were also found in the A9-vt, though in greater numbers. As the A8-RRF emerged, a few double-labeled cells were found in this field, but relatively more were found in the caudal extensions of the A9-dt and A9-vt. Few to no double-labeled cells were found in the A10-VTA at all levels.

Interstitial nucleus of the posterior limb of the anterior commissure (IPAC)—A moderate number of cells were double-labeled following injections into the IPAC. Double-labeled cells emerged mid-way through the midbrain, and spread along the medial A9-dt. There were a moderate number of double-labeled cells located in the lateral A10-VTA, rostrally to caudally, and in the A8-RRF, mostly in the medial aspect of this field. Few to no double-labeled cells were found in the caudal most A8-RRF.

Other brain regions containing double-labeled cells

In addition to the ventral midbrain, we examined regions containing TH-positive cells in the prefrontal cortex, the ventricular zone of the third and fourth ventricles, the zona incerta (A13), posterior hypothalamus (A10), periaqueductal gray (rostral A10), and pons (including the dorsal raphe, caudal A10 group, locus coeruleus, A6–A7 groups) for evidence of double-labeled cells. Double-labeled cells were only seen in the main locus coeruleus (A7) and A5 group. Retrograde injections into all of the amygdaloid nuclei, except for the amygdalostriatal

area, resulted in bilaterally double-labeled cells in the A5 and A7 groups, which are noradrengeric (Kemper et al., 1987).

Anterograde results

Anterogradely labeled terminal fiber patterns were similar for injections in the medial A9-SNpc (J15FR) and the A8-RRF (J16FS, J19FS), consistent with retrograde results. Terminal fibers were most densely distributed in the CeM and amygdalostriatal area (Fig. 10). A somewhat sparser distribution of fibers was seen in the IPAC, while the CeLcn was devoid of labeled fibers following all injection sites. Very fine, beaded labeled fibers were lightly concentrated and scattered throughout all of the nuclei of the amygdala proper. Because of their thin caliber and diffuse distribution, labeled fibers in the basolateral nuclear region were only appreciated at high power (10× or greater) (Fig. 10). The injection in the lateral A9-SNpc (J21FS) resulted in a pattern of anterograde labeling similar to the previously described injections, though uniformly less dense. The injection site in the ventral tier of the A9 group (J20FR) did not result in labeled fibers in the amygdala.

DISCUSSION

Summary of findings

Following all injection sites into the amygdala proper and extended amygdala, the majority of retrograde-labeled cells with TH-immunoreactivity were concentrated at the central to caudal levels of the midbrain, with fewer labeled cells found rostrally. In general, different injections into the same nuclei resulted in the same general pattern of retrograde labeling, and among specific injection sites there was little difference in the pattern of retrograde-labeled cells resulting from single-labeling and double-labeling experiments. A somewhat surprising finding was that the A10-VTA was not the sole, or main, input to any of the amygdala or extended amygdala subregions, with other subregions making a relatively greater contribution, as described below.

Input from A10-ventral tegmental area—Compared to other dopamine subpopulations, there was relatively less input from A10-VTA following all injection sites (Table 2, Fig. 11). Still, all nuclei except for the amygdalostriatal area received some innervation from the A10-VTA, mostly from the lateral part. Compared to the extended amygdala, the “amygdala proper” as a whole received relatively more input from the A10-VTA. Within the amygdala proper, the magnocellular subdivisions of the basal (Bmc) and accessory basal (ABmc) nucleus received the greatest density of A10-VTA input. In contrast, the parvicellular divisions of these nuclei (ABpc and Bpc) received almost no input from A10-VTA. The extended amygdala had proportionately less input from the A10-VTA than the magnocellular divisions of the “amygdala proper,” and the amygdalostriatal area received almost no input from A10-VTA. There were few to no double-labeled cells in more rostral or caudal components of the A10 group, such as the periaqueductal grey (PAG) and dorsal raphe (DR), following any injection site, an interesting finding that will be discussed in the following sections.

Input from A9-substantia nigra, pars compacta—The A9 group as a whole provided substantial DA-ergic innervation to most of the injected amygdala nuclei, with much of the innervation arising from the dorsal tier (Fig. 11). Only the Bpc and ABpc received little to no input from the A9 group, the exception being case J15FS, which received input from both the A9 ventral and dorsal tiers. This injection was placed at the caudal edge of the Bpc, and the higher density of double-labeled cells likely reflects the higher density of TH-fibers at this level (Akil and Lewis, 1993) (unpublished observations). While all other amygdala regions received A9-dt input, only a few nuclei received input from the ventral tier, based on our retrograde results. These included: CeM, amygdalostriatal area, and ABmc. In the case of the

ABmc, encroachment of the injection sites into the CeM, or into intercalated islands interposed between the CeM and ABmc, may be a possible reason for double-labeled cells in the A9-vt. We are unable to rule out this possibility in our material at present. The CeM, amygdalostriatal area and Bmc continued to receive input from the caudal extension of the A9-dt, while the CeM and amygdalostriatal area received input from the caudal A9-vt, as well.

With the exception of Bpc and ABpc, which receive almost exclusive innervation from the A8-RRF (see below), the A9-SNpc innervation to both the "amygdala proper" and extended amygdala arose from the entire medio-lateral extent of the A9-dt. In general, a ventral-dorsal and medio-lateral topography was observed, such that injections in the more ventral Bmc and ABmc received relatively greater innervation from the medial A9-dt, whereas the CeM and amygdalostriatal area received more input from the lateral A9-dt. The IPAC, a more rostral component of the extended amygdala, received relatively more innervation from the medial A9-dt than the lateral A9-dt. This suggests that more rostromedial aspects of the extended amygdala may receive inputs from the medial aspects of A9-dt, while more caudolateral components receive inputs from more lateral DA cell groups. More retrograde and anterograde studies are needed to determine whether this is the case.

Input from A8-retrorubral field—The A9-dt merges laterally and caudally with the A8-RRF, and all of the nuclei received substantial innervation from the A8-RRF (Fig. 11). Most of the double-labeled cells spanned the medio-lateral extent of the A8-RRF. In general, the A8-RRF provided more input to the extended amygdala than the amygdala proper, with the exception of the amygdalostriatal area. Our anterograde injections placed in the medial A8-RRF confirmed these findings. In addition, though most of the Bpc and ABpc received relatively less dopaminergic innervation overall, compared to the rest of the nuclei, the small input they did receive arose mostly from A8-RRF. Again, case J15FS (Bpc), placed in the caudal pole of Bpc, had relatively more double-labeled cells, consistent with the higher concentration of TH-fibers in this region.

Comparisons of inputs to extended amygdala and amygdala proper—Overall, injections into the extended amygdala resulted in relatively more double-labeled cells, compared to the injections in the amygdala proper. These retrograde results are consistent with our anterograde studies, which showed a much denser terminal field over the extended amygdala structures following injections in the medial A9 group and A8-RRF. For the extended amygdala injections, relatively double-more labeled cells were found in the A9-dt, with the next highest concentration in the A8-RRF, and relatively fewer double-labeled cells in the A10-VTA (Table 2). For the Bmc and ABmc of the amygdala proper, double-labeled cells were distributed relatively equally between the A10-VTA, A9-dt, and A8-RRF. The ABpc and Bpc stood out as receiving most of their input from the A8-RRF.

Injections into the two subdivisions of the central nucleus resulted in strikingly different numbers of labeled cells. While injections into the medial division of the central nucleus (CeM) resulted in numerous double-labeled cells in the dorsal and ventral tiers, two injections into the lateral division (CeLcn) resulted in virtually no single-labeled cells in the ventral midbrain, despite many single-labeled cells in known afferent sources such as the parabrachial nucleus (not shown). This pattern was also confirmed with antero-grade injections resulting in labeled fibers only in the CeM (Fig. 10). These results indicate that the dense TH-positive fibers seen in the CeLcn (Freedman and Shi, 2001) arise from TH-positive cell groups outside the ventral midbrain.

Technical considerations

Evaluating nondopaminergic pathways and autofluorescence—Non-dopaminergic projections have been reported in the rat (Swanson, 1982). Our control experiments in animals with and without tracer injections revealed a large number of small, auto-fluorescing cells seen under both the red, 546 and 596 cubes, and the green, 488 cube. Though these auto-fluorescing cells were indistinguishable from the single, tracer-labeled cells, they were significantly different from the TH-labeled dopaminergic cells. Under the 488 cube, these auto-fluorescing cells were often located in the substantia nigra pars reticulata, were smaller, and had a golden color, as opposed to the larger, bright green cells detected with fluorophor-tagged secondary antibody. Because of the auto-fluoresence of these non-TH-containing cells, we were unable to make any conclusions about non-dopaminergic projections within the primate. However, the relatively low number of truly double-labeled cells, their distinct appearance in contrast to the autofluorescent cells, and their identical distribution to the pattern of single-labeled cells seen in DAB stained sections, makes it unlikely that our TH-containing projection neurons are false positives. Finally, our anterograde studies showed that tracer injections into A9-SNpc regions containing truly double-labeled cells resulted in labeled fibers in the amygdala, while injections placed in regions containing only autofluorescing cells (e.g. the SNpr and lateral ventral tier) had no anterograde-labeled fibers in the amygdala.

Patterns of cell labeling—Analysis of most of our injection sites revealed relatively low quantities of double-labeled cells within the ventral midbrain. Comparing other primate studies giving quantitative information on dopaminergic inputs to the amygdala, our results are similar (Norita and Kawamura, 1980). Looking at retrograde studies focusing on DA inputs to nearby or related areas, such as the hippocampus, entorhinal cortex or pre-frontal cortex, our results appear to reflect the size of our injection sites. For example, a study using large injection sites to examine dopaminergic inputs to the hippocampus showed more labeled cells than our study, while a study with smaller, discrete injections into the entorhinal cortex had as many, or fewer, labeled cells as our study (Amaral and Cowan, 1980; Insausti et al., 1987). In addition, our injections into the amygdala proper resulted in relatively fewer double-labeled cells than injections into the extended amygdala, a finding reflecting the differential terminal fiber distribution in the two areas, as revealed by our antero-grade tracer studies (Fig. 10).

Fibers of passage—Retrograde studies provide a broad overview of potential afferent structures, and can be combined with biomarkers such as TH to characterize transmitter-specific pathways. A concern for all retrograde tracer studies, however, is the possibility of tracer uptake and transport by fibers of passage, leading to false positive results (Halperin and LaVail, 1975; Nance and Burns, 1990). This is particularly relevant for injections into extended amygdala structures, which contains fibers passing from the amygdala proper to the thalamus, hypothalamus and brainstem as part of the ventral amygdalofugal pathway. A few different techniques were used to avoid this problem. We used slow, pressure injections of tracer through small bore pipettes in order to avoid tissue necrosis or damage that would lead to tracer uptake by fibers (Nance and Burns, 1990; Schmued et al., 1990; Vercelli et al., 2000). We also examined cases with injections into the extended amygdala for extraneous cell labeling indicative of fiber uptake, and saw no single-labeled cells or fibers in the mediodorsal thalamus, for example (Porrino et al., 1981; Aggleton and Mishkin, 1984; Russchen et al., 1987). Fibers of passage significantly contaminated during injections into the extended amygdala would have also resulted in more retrograde labeling in the A10-VTA, due to fibers running from the Bmc and ABmc to the A10-VTA. This did not appear to be the case, as the extended amygdala structures appeared to receive little input from the A10-VTA. Indeed, two injection sites in the CeLcn resulted in no single-labeled cells in the midbrain, but numerous single-labeled cells in the parabrachial nucleus, as expected, suggesting tracer uptake without disturbance of fibers of passage. Finally, cases with injections into nearby fiber tracts, such as the anterior

commissure and external capsule resulted in few labeled cells, indicating that our pressure injection technique minimized significant tracer uptake by fibers tracts. Complementary antero-grade studies were also used to interpret retrograde results, and to examine the density and scope of terminal fields in specific amygdala subregions.

Comparisons among species

A10-VTA input in the rat and primate—A major finding in our study is the substantially lower contribution from the A10-VTA to the primate amygdala, compared to the contribution from the A9 and the A8-RRF. Studies in the rat have classically defined the "mesolimbic pathway" as projecting from the A10-VTA to limbic areas including the amygdala and nucleus accumbens. In our study, while the A10-VTA, in particular the lateral VTA, provides dopamine to the primate amygdala, the A9-dt and A8-RRF appear to provide significantly more innervation.

Taking a closer look at the literature in the rat, the idea of a discrete mesolimbic pathway appears to be an over-generalization, and may be even more so in the primate. In general, the studies conducted in the rat have looked at either the amygdala proper only, the extended amygdala only, or projections from only one DAergic source. Without more comprehensive rodent studies, it is difficult to make accurate comparisons between the different areas of the amygdala and the subpopulations of the DAergic midbrain. Looking at nuclei of the amygdala proper, our study suggests that a lower proportion of double-labeled cells in the lateral A10-VTA contribute to the Bmc and ABmc in the primate, compared to the rat, which receives about 50% of its dopamine from the lateral A10-VTA (Fallon et al., 1978). A combined retrograde and anterograde tracer study in rat also verified that amygdalar DA arises from the A10-VTA, though the data in the A9 group was uninterpretable due to spread of the retrograde injection to the caudoputamen and globus pallidus (Swanson, 1982).

In our review of the literature, three papers examining the afferents to the primate amygdala using a tracer method were found (Aggleton et al., 1980; Mehler, 1980; Norita and Kawamura, 1980). Because the primary objective of these papers was to detail the subcortical afferents to the monkey amygdala, and not to determine dopaminergic projections, none of these studies co-labeled with tyrosine hydroxylase. These studies included some injections confined to specific amygdalar nuclei, but also large injections that spread beyond single nuclei (Aggleton et al., 1980; Mehler, 1980; Norita and Kawamura, 1980). In contrast, our study used small injection sites confined to specific nuclei that covered a smaller proportion of the amygdala, in order to derive nuclei-specific conclusions about the dopaminergic projections to the primate amygdala. Though a direct comparison is difficult, results from the primate literature, in general, agreed with our results showing modest A10-VTA input, with additional A9-SNpc and A8-RRF input. Norita and Kawamura confirmed A10-VTA, but also A9-SNpc and A8-RRF, input following a nuclei-specific injection in the medial nucleus (Norita and Kawamura, 1980). The paper by Aggleton et al. described a few cells in the A10-VTA following injections into the amygdala proper, and also a few single-labeled cells in the A9-SNpc following injections covering the central and me-dial nuclei. A8-RRF labeling was not reported. Mehler described input arising mostly from the A10-VTA group to elements of the amygdala proper, and specifically mentioned a lack of A8-RRF input. Projections from the A9-SNpc were not discussed due to a potential problem of false-positives in that study (Mehler, 1980). Our results showing a lack of input from the A10-VTA to the parvicellular divisions of the accessory basal and basal nuclei (ABpc and Bpc) could not be compared to other primate studies, since nuclei subdivision-specific studies could not be found.

In the rat central extended amygdala, an extensive study using retrograde tracers showed that most of the DA-containing projections to the central nucleus, amygdalostriatal area, and IPAC arose from A10 catecholamine groups including the A10-VTA, but also the PAG and DR, with

far less innervation from the A9-SNpc or A8-RRF (Hasue and Shammah-Lagnado, 2002). Other studies, however, in the rat and cat central nucleus reported inner-vation from A9-dt, in addition to input from the A10-VTA, though the TH-status of these sources was not confirmed (Meibach and Katzman, 1981; Ottersen, 1981; Russchen, 1982). In the rat, Ottersen demonstrated a lack of A10-VTA input to the medial nucleus following single-labeling studies for retrograde tracer (Ottersen, 1981).

The monkey literature shows a sparse input from the A10-PAG, with a more dense input from the A10-DR, following injections into the amygdala proper or the central or medial nucleus (Aggleton et al., 1980; Mehler, 1980; Norita and Kawamura, 1980). However, because dopaminergic cells form only one component of cells within the PAG and DR, and none of these studies co-labeled with TH, conclusions about the dopaminergic status of these inputs cannot be made. In our study, single (tracer) labeled sections did reveal a number of labeled cells in the A10-PAG and A10-DRN, but double-labeling studies indicate that they do not appear to provide significant dopaminergic input to any amygdala nuclei in the primate. Thus, in the primate, elements of the extended amygdala including the central nucleus, medial nucleus, amygdalostriatal area and IPAC receive little input from the A10-VTA, and no input from TH-positive cells of the A10-PAG or A10-DR, a finding that may represent a species difference from that in the rat. In contrast, elements of the amygdala proper, in particular the Bmc and ABmc, receive a moderate input from the lateral A10-VTA, similar to in the rat.

A9-SNpc input in the rat and primate—Our study suggests that the A9-dt is a major source of dopamine for both the amygdala proper and extended amygdala in the primate. The rat literature shows conflicting data with respect to contributions from the A9-SNpc. In general, rat studies show input from the medial A9-SNpc, while our primate study shows innervation arising from the entire medio-lateral extent of the A9-SNpc. In the rat, lesions to the medial A9 group led to a 50% decrease in DA to the amygdala proper, the central and medial nuclei, with lesions to the lateral A10-VTA accounting for the other 50% (Fallon et al., 1978). However, one tracer study in rat demonstrated a lack of A9-SNpc input to the amygdala proper, while another demonstrated TH-positive input from the expanse of A9-dt following a large injection site covering the entire amygdala proper and central nucleus, a finding that is closest to our results (Ottersen, 1981; Loughlin and Fallon, 1983). Our study shows that the magnocellular divisions of the basal and accessory basal nuclei in the monkey do receive input from the medial A9 group, but that significant innervation also arises from the entire medio-lateral extent of the A9-dt. Within the primate literature, an injection into the lateral nucleus and large injections into the amygdala proper yielded single-labeled cells within the A10-VTA only, though these cells were not examined for TH-immunoreactivity, while another study did not comment on A9-SNpc input due to a possibility of false positives (Aggleton et al., 1980; Mehler, 1980; Norita and Kawamura, 1980).

Within the rat extended amygdala, a double-labeling study of discrete injections into the central nucleus, amygdalostriatal area and IPAC showed relatively sparse TH-positive inputs from the A9-dt, a finding that differs from our study in the primate (Hasue and Shammah-Lagnado, 2002). A few tracer studies have shown projections from the A9-dt to the central nucleus in the rat and the cat, though none of these studies examined for TH-immunore-activity (Meibach and Katzman, 1981; Ottersen, 1981; Russchen, 1982). In primates, the only available studies are single labeling retrograde studies, which did show inputs arising from the A9-SNpc to the central and medial nuclei (Aggleton et al., 1980; Norita and Kawamura, 1980). In our present results, the extended amygdala received TH-positive input from across the entirety of the A9-dorsal tier. Overall, the input from the A9-dt to the extended amygdala and amygdala proper appears more extensive in the primate, than in the rat or the cat.

Prior studies addressing input from the A9-vt were not found. Our present results indicate that the medial ventral tier forms a modest input to the medial subdivision of the CeN, the amygdalostriatal area, and possibly the ABmc.

A8-RRF input in the rat and primate—Like the adjacent A9-dt, the A8-RRF also represents a significant source of DA for the primate amygdala proper and extended amygdala. Only one study in the rat addressed this area. Anterograde tracer injections placed in the A8-RRF resulted in labeled fibers in the central nucleus and amygdalostriatal area (Deutch et al., 1988). Information on the inputs from the A8-RRF in the primate was not supplied in existing primate studies, with the exception of the paper by Mehler specifically mentioning a lack of A8-RRF input (Aggleton et al., 1980; Mehler, 1980; Norita and Kawamura, 1980). Our study shows that all nuclei of the primate amygdala receive input from the A8-RRF, and this area represents a significant source of DA for both the extended amygdala and amygdala proper. The relative innervation from the A8-RRF group, compared to the A10-VTA, appears to be more extensive in the primate than in the rat.

Other amygdaloid nuclei

Because our study was aimed at understanding nuclei-specific projections, we used small injections that did not cover the entirety of the amygdala. Areas of the basal nucleus, the entire lateral nucleus, and the BNST were not injected. There is little information on the sources of dopa-mine to these areas in the primate, however, immunostaining for TH shows low immunoreactivity in the lateral nucleus, with greater staining in the BNST (Freedman and Shi, 2001) (unpublished observations). Norita and Kawamura described one injection centered in the lateral nucleus with modest leakage into the dorsal basal nucleus that resulted in a few single-labeled cells in the A10-VTA, but no cells in other dopaminergic areas (Norita and Kawamura, 1980). No information on projections to the primate BNST was found, a potential topic for future work.

Anatomic areas for dopamine regulation

Based on our present results, the DAergic input from the ventral midbrain to the primate amygdala is broader than the input to the rat amygdala, and likely reflects the expansion of the primate midbrain. The primate midbrain DA system is more expansive in all planes (rostrocaudal, mediolateral, and dorsoventral) than that in the rat, while the human system is the most expansive of all (Bjorklund and Dunnett, 2007). The rat midbrain contains 40,000–45,000 TH-positive cells bilaterally among the A8–A10 groups, with 50% located in the A9 group. In the monkey, >70% of its 160,000–320,000 TH-positive cells are located in the A9 group. 10–11% of the cells are located in the A8 group, while 18% are in the VTA (Hirsch et al., 1992; Francois et al., 1999). In the human, the proportion of dopaminergic neurons in the A9 group is similar to that in the monkey, but the total number of neurons is 400,000–600,000. Because of the expansion of the A9 group, and the expansion of input to the amygdala from this area, the A9 group may be a more important subregion for regulating dopaminergic input to the amygdala in higher species.

The present results, along with our previous work, raise the possibility that a closed-loop nigro–amygdala–nigral circuit may contribute to the regulation of DA to the primate amygdala. In the primate, the extended amygdala sends projections back to midbrain dopaminergic groups, suggesting that the extended amygdala may be involved in afferent regulation of its DAergic efferents (Fudge and Haber, 2000, 2001). The amygdalostriatal area and medial subdivision of the central nucleus project mostly to A9-dt, with a few projections to the ventral tier as well (Fudge and Haber, 2000, 2001). This circuitry is especially interesting given our results suggesting that these components of the extended amygdala receive denser DAergic input than the amygdala proper, and are among the few nuclei that also receive ventral tier inputs.

Our finding that the A9-dt and A8-RRF provide much of the DA to the primate amygdala is consistent with other studies showing projections from these dopamine sub-populations to other primate limbic structures. In the primate, the core of the nucleus accumbens receives input from the A10-VTA, but also from the A9-dt and the A8-RRF (Francois et al., 1999; Haber et al., 2000). The entorhinal cortex in the primate, another area reciprocally connected with the amygdala, also receives a modest dopaminergic input from the A9-SNpc, though the primate hippocampus receives input exclusively from the A10-VTA (Amaral and Cowan, 1980; Insausti et al., 1987). A comprehensive study of the dopaminergic inputs to the primate PFC also revealed the A9-dt and A8-RRF as major sources of DA for different areas of the PFC, with relatively less input from the A10-VTA group (Williams and Goldman-Rakic, 1998). The amygdala and areas of the PFC are known to have reciprocal connections in the rat and primate (McDonald, 1991; Carmichael and Price, 1995; McDonald et al., 1996; Ghashghaei and Barbas, 2002). In rats, the PFC exerts inhibition onto the amygdala that can be attenuated by dopamine (Rosenkranz and Grace, 1999). In turn, the amygdala has both inhibitory and excitatory influences on the PFC that can be reversed with dopamine (Floresco and Tse, 2007). Thus, contrary to the rat, where limbic regions receive near exclusive A10-VTA input, several nodes of the primate limbic system receive additional input from the A9-dt and A8-RRF. Because of the convergence of the A9-dt and A8-RRF onto components of the primate limbic system, and the importance of dopamine to each of these areas, A9-dt and A8-RRF represent another key component of the primate limbic system.

Functional implications

Studies in rat show that dopamine neurotransmission is prolonged in the amygdala, suggesting that regulation may occur through volume transmission, rather than classical wiring transmission (Garris and Wightman, 1994). During volume transmission, neurotransmitters travel beyond the synaptic cleft, exerting an effect at more distant locations, on more than one cell, and for a longer period of time (Zoli et al., 1998). Within the rat amygdala proper, voltammetric measurement of evoked extracellular DA has confirmed delayed clearance of DA, compared to that in the striatum and nucleus accumbens (Garris and Wightman, 1994; Jones et al., 1995). Adjusting the rate of DA clearance for the density of TH terminals reveals a 10-fold less clearance rate in the basal nucleus, compared to in the nucleus accumbens, striatum and PFC (Garris and Wightman, 1994). Because learning is a complex process involving different types of cells, and occurring with repeated exposure over a prolonged period of time, the spatio-temporal kinetics of volume transmission may be a feature enabling dopamine to sustain fear learning (Zoli et al., 1998).

Our anatomic results appear consistent with the idea that dopamine works through volume transmission within the amygdala. The wide dispersal of labeled fibers in the amygdala proper following anterograde injections supports the idea that innervation of these “cortical-like” nuclei is organized to allow DA diffusion over long distances. Moreover, in primates, dopamine transporter (DAT) mRNA is relatively low in the A9-dt, and abundant in the A9-vt (Haber et al., 1995). Because our results show that the primate amygdala receives most of its dopamine from the A9-dt, relatively low amounts of DAT may contribute to volume transmission by slowing the clearance of DA. Indeed, staining of the primate amygdala for DAT has revealed little immunoreactivity outside of the CeM and amygdalostriatal area (Freedman and Shi, 2001) (unpublished observations). Thus, our findings of widely dispersed terminal fibers, and input from dorsal tier neurons lacking classical uptake mechanisms support the idea of volume transmission occurring within the amygdala proper. Further research on the kinetics of dopamine in the primate amygdala is needed to confirm this.

The unique ability of dopamine to work through volume transmission may represent a mechanism through which the amygdala is able to participate in sustained activities, such as

fear learning. This mechanism may also provide insight into the persistent or exaggerated fear learning associated with affective disorders. For instance, repeated exposure to stressful stimuli may lead to increased DA release, which in the amygdala is coupled with relatively delayed uptake. Sustained dopamine transmission may result in hypersensitivity to ongoing fear learning, which may underlie the related symptoms of anxiety, ruminative thinking, and negative thought patterns in vulnerable individuals.

Acknowledgments

This work was supported by 2R01 MH62391 (JF), and a Clinical and Translational Science Institute Young Investigator award (National Center for Research Resources (NCRR) a component of the National Institutes of Health (NIH) and NIH Roadmap for Medical Research) TL1 RR024135 (YTC). The project described is solely the responsibility of the authors and do not necessarily represent the official view of the NCRR or NIH. Information on the NCRR is available at http://www.ncrr.nih.gov. Information on Re-engineering the Clinical Research Enterprise can be obtained from http://nihroadmap.nih.gov/clinicalresearch/overview-traslational.asp. We thank Ms. Kyeesha Becoats for her excellent histologic support and Ms. Tracy Bubel and Linda Callahan, PhD for assistance with fluorescent and confocal microscopy, respectively.

Abbreviations

III N	cranial nerve III
A8-RRF	A8-retrorubral field
A9-dt	A9-dorsal tier of substantia nigra
A9-vt	A9-ventral tier of substantia nigra
A10-VTA	A10-ventral tegmental area
AAA	anterior amygdaloid area
ABbs	accessory basal nucleus, sulcal subdivision
ABmc	accessory basal nucleus, magnocellular subdivision
ABpc	accessory basal nucleus, parvicellular subdivision
AC	anterior commissure
AChE	acetylcholinesterase
AHA	amygdalohippocampal area
Aq	aqueduct
Astr	amygdalostriatal area
Bi	basal nucleus, intermediate subdivision
Bmc	basal nucleus, magnocellular subdivision
BNST	bed nucleus of the stria terminalis
Bpc	basal nucleus, parvicellular subdivision
C	caudate nucleus
CaBP	Calbindin-D28k
CeLcn	central nucleus, lateral core subdivision
CeM	central nucleus, medial subdivision
CL	claustrum
CoA	anterior cortical nucleus

CoP	posterior cortical nucleus
DA	dopamine
DAT	dopamine transporter
EC	external capsule
GPe	globus pallidus, external segment
H	hippocampus
IC	internal capsule
IPAC	interstitial nucleus of the posterior limb of the anterior commissure
L	lateral nucleus
M	medial nucleus
ML	medial lemniscus
NGS	normal goat serum
O	optic tract
P	putamen
PAC	periamygdaloid cortex, subdivisions I-III
PAG	periaqueductal grey
PB	phosphate buffer
PFC	pre-frontal cortex
RN	red nucleus
SCP	superior cerebellar peduncle
SNpr	substantia nigra, pars reticulate
TH	tyrosine hydroxylase
TX	Triton-X
V	ventricle

REFERENCES

Aggleton JP, Mishkin M. Projections of the amygdala to the thalamus in the cynomolgus monkey. J Comp Neurol 1984;222:56–68. [PubMed: 6321564]

Aggleton JP, Burton MJ, Passingham RE. Cortical and subcortical afferents to the amygdala of the rhesus monkey (*Macaca mulatta*). Brain Res 1980;190:347–368. [PubMed: 6768425]

Akil M, Lewis DA. The dopaminergic innervation of monkey entorhinal cortex. Cereb Cortex 1993;3:533–550. [PubMed: 7907902]

Alheid GF. Extended amygdala and basal forebrain. Ann N Y Acad Sci 2003;985:185–205. [PubMed: 12724159]

Alvarez RP, Biggs A, Chen G, Pine DS, Grillon C. Contextual fear conditioning in humans: cortical-hippocampal and amygdala contributions. J Neurosci 2008;28:6211–6219. [PubMed: 18550763]

Amaral DG, Cowan WM. Subcortical afferents to the hippocampal formation in the monkey. J Comp Neurol 1980;189:573–591. [PubMed: 6769979]

Amaral DG, Bassett JL. Cholinergic innervation of the monkey amygdala: an immunohistochemical analysis with antisera to choline acetyltransferase. J Comp Neurol 1989;281:337–361. [PubMed: 2703552]

Amaral, DG.; Price, JL.; Pitkanen, A.; Carmichael, ST. The Amygdala: neurobiological aspects of emotion, memory, and mental dysfunction. Wiley-Liss; Wilmington, DE: 1992. Anatomical organization of the primate amygdaloid complex; p. 1-66.

Bjorklund A, Dunnett SB. Dopamine neuron systems in the brain: an update. Trends Neurosci 2007;30:194–202. [PubMed: 17408759]

Carmichael ST, Price JL. Limbic connections of the orbital and medial prefrontal cortex in macaque monkeys. J Comp Neurol 1995;363:615–641. [PubMed: 8847421]

DeOlmos, JS. Amygdala. In: Paxinos, G., editor. The human nervous system. Academic Press; San Diego, CA: 1990. p. 583-710.

Deutch AY, Goldstein M, Baldino F Jr, Roth RH. Telencephalic projections of the A8 dopamine cell group. Ann N Y Acad Sci 1988;537:27–50. [PubMed: 2462395]

Fadok JP, Dickerson TM, Palmiter RD. Dopamine is necessary for cue-dependent fear conditioning. J Neurosci 2009;29:11089–11097. [PubMed: 19741115]

Fallon JH, Koziell DA, Moore RY. Catecholamine innervation of the basal forebrain. II. Amygdala, suprarhinal cortex and entorhinal cortex. J Comp Neurol 1978;180(3):509–532. [PubMed: 659673]

Floresco SB, Tse MT. Dopaminergic regulation of inhibitory and excitatory transmission in the basolateral amygdala-prefrontal cortical pathway. J Neurosci 2007;27:2045–2057. [PubMed: 17314300]

Francois C, Yelnik J, Tande D, Agid Y, Hirsch EC. Dopaminergic cell group A8 in the monkey: anatomical organization and projections to the striatum. J Comp Neurol 1999;414:334–347. [PubMed: 10516600]

Freedman LJ, Shi C. Monoaminergic innervation of the macaque extended amygdala. Neuroscience 2001;104:1067–1084. [PubMed: 11457591]

Fudge J, Haber S. Defining the caudoventral striatum in primates: cytoarchitectural and histochemical features. J Neurosci 2002;22:10078–10082. [PubMed: 12451107]

Fudge JL, Haber SN. The central nucleus of the amygdala projection to dopamine subpopulations in primates. Neuroscience 2000;97:479–494. [PubMed: 10828531]

Fudge JL, Haber SN. Bed nucleus of the stria terminalis and extended amygdala inputs to dopamine subpopulations in primates. Neuroscience 2001;104:807–827. [PubMed: 11440812]

Fudge JL, Tucker T. Amygdala projections to central amygdaloid nucleus subdivisions and transition zones in the primate. Neuroscience 2009;159:819–841. [PubMed: 19272304]

Fudge JL, Breitbart MA, McClain C. Amygdaloid inputs define a caudal component of the ventral striatum in primates. J Comp Neurol 2004;476:330–347. [PubMed: 15282709]

Fuxe K, Hokfelt T, Ungerstedt U. Morphological and functional aspects of central monoamine neurons. Int Rev Neurobiol 1970;13:93–126.

Garris PA, Wightman RM. Different kinetics govern dopaminergic transmission in the amygdala, prefrontal cortex, and striatum: an in vivo voltammetric study. J Neurosci 1994;14:442–450. [PubMed: 8283249]

Geneser-Jensen FA, Blackstad TW. Distribution of acetyl cholinesterase in the hippocampal region of the guinea pig. I. Entorhinal area, parasubiculum, and presubiculum. Z Zellforsch Mikrosk Anat 1971;114:460–481. [PubMed: 5550728]

German DC, Manaye KF, Sonsalla PK, Brooks BA. Midbrain dopaminergic cell loss in Parkinson's disease and MPTP-induced parkinsonism: sparing of calbindin-D28k-containing cells. Ann N Y Acad Sci 1992;648:42–62. [PubMed: 1353337]

Ghashghaei HT, Barbas H. Pathways for emotion: interactions of prefrontal and anterior temporal pathways in the amygdala of the rhesus monkey. Neuroscience 2002;115:1261–1279. [PubMed: 12453496]

Greba Q, Kokkinidis L. Peripheral and intraamygdalar administration of the dopamine D1 receptor antagonist SCH 23390 blocks fear-potentiated startle but not shock reactivity or the shock sensitization of acoustic startle. Behav Neurosci 2000;114:262–272. [PubMed: 10832788]

Greba Q, Gifkins A, Kokkinidis L. Inhibition of amygdaloid dopamine D2 receptors impairs emotional learning measured with fear-potentiated startle. Brain Res 2001;899:218–226. [PubMed: 11311883]

Guarraci FA, Frohardt RJ, Kapp BS. Amygdaloid D1 dopamine receptor involvement in Pavlovian fear conditioning. Brain Res 1999;827:28–40. [PubMed: 10320690]

Guarraci FA, Frohardt RJ, Falls WA, Kapp BS. The effects of intra-amygdaloid infusions of a D2 dopamine receptor antagonist on Pavlovian fear conditioning. Behav Neurosci 2000;114:647–651. [PubMed: 10883814]

Haber SN, Fudge JL, McFarland N. Striatonigrostriatal pathways in primates form an ascending spiral from the shell to the dorsolateral striatum. J Neurosci 2000;20:2369–2382. [PubMed: 10704511]

Haber SN, Ryoo H, Cox C, Lu W. Subsets of midbrain dopaminergic neurons in monkeys are distinguished by different levels of mRNA for the dopamine transporter: comparison with the mRNA for the D2 receptor, tyrosine hydroxylase and calbindin immuno-reactivity. J Comp Neurol 1995;362:400–410. [PubMed: 8576447]

Halperin JJ, LaVail JH. A study of the dynamics of retrograde transport and accumulation of horseradish peroxidase in injured neurons. Brain Res 1975;100:253–269. [PubMed: 53088]

Hasue RH, Shammah-Lagnado SJ. Origin of the dopaminergic innervation of the central extended amygdala and accumbens shell: a combined retrograde tracing and immunohistochemical study in the rat. J Comp Neurol 2002;454:15–33. [PubMed: 12410615]

Hirsch E, Graybiel AM, Agid YA. Melanized dopaminergic neurons are differentially susceptible to degeneration in Parkinson's disease. Nature 1988;334:345–348. [PubMed: 2899295]

Hirsch EC, Mouatt A, Thomasset M, Javoy-Agid F, Agid Y, Graybiel AM. Expression of calbindin D_{28K}-like immunoreactivity in catecholaminergic cell groups of the human midbrain: normal distrubution and distrubution in Parkinson's disease. Neurodegeneration 1992;1:83–93.

Insausti R, Amaral DG, Cowan WM. The entorhinal cortex of the monkey: III. Subcortical afferents. J Comp Neurol 1987;264:396–408. [PubMed: 3680636]

Jones SR, Garris PA, Kilts CD, Wightman RM. Comparison of dopamine uptake in the basolateral amygdaloid nucleus, caudateputamen, and nucleus accumbens of the rat. J Neurochem 1995;64:2581–2589. [PubMed: 7760038]

Kemper CM, O'Connor DT, Westlund KN. Immunocytochemical localization of dopamine-beta-hydroxylase in neurons of the human brain stem. Neuroscience 1987;23:981–989. [PubMed: 3437997]

Kienast T, Hariri AR, Schlagenhauf F, Wrase J, Sterzer P, Buchholz HG, Smolka MN, Grunder G, Cumming P, Kumakura Y, Bartenstein P, Dolan RJ, Heinz A. Dopamine in amygdala gates limbic processing of aversive stimuli in humans. Nat Neurosci 2008;11:1381–1382. [PubMed: 18978778]

Lavoie B, Parent A. Dopaminergic neurons expressing calbindin in normal and parkinsonian monkeys. Neuroreport 1991;2(10):601–604. [PubMed: 1684519]

Loughlin SE, Fallon JH. Dopaminergic and non-dopaminergic projections to amygdala from substantia nigra and ventral tegmental area. Brain Res 1983;262:334–338. [PubMed: 6839161]

Martin LJ, Powers RE, Dellovade TL, Price DL. The bed nucleus-amygdala continuum in human and monkey. J Comp Neurol 1991;309:445–485. [PubMed: 1918444]

McDonald AJ. Organization of amygdaloid projections to the prefrontal cortex and associated striatum in the rat. Neuroscience 1991;44:1–14. [PubMed: 1722886]

McDonald AJ, Mascagni F, Guo L. Projections of the medial and lateral prefrontal cortices to the amygdala: a *Phaseolus vulgaris* leucoagglutinin study in the rat. Neuroscience 1996;71:55–75. [PubMed: 8834392]

Mehler WR. Subcortical afferent connections of the amygdala in the monkey. J Comp Neurol 1980;190:733–762. [PubMed: 6772695]

Meibach RC, Katzman R. Origin, course and termination of dopaminergic substantia nigra neurons projecting to the amygdaloid complex in the cat. Neuroscience 1981;6:2159–2171. [PubMed: 7329546]

Nader K, LeDoux JE. Inhibition of the mesoamygdala dopaminergic pathway impairs the retrieval of conditioned fear associations. Behav Neurosci 1999;113:891–901. [PubMed: 10571473]

Nance DM, Burns J. Fluorescent dextrans as sensitive anterograde neuroanatomical tracers: applications and pitfalls. Brain Res Bull 1990;25:139–145. [PubMed: 1698517]

Norita M, Kawamura K. Subcortical afferents to the monkey amygdala: an HRP study. Brain Res 1980;190:225–230. [PubMed: 6769534]

Oaksford M, Stenning K. Reasoning with conditionals containing negated constituents. J Exp Psychol Learn Mem Cogn 1992;18:835–854. [PubMed: 1385619]

Ottersen OP. Afferent connections to the amygdaloid complex of the rat with some observations in the cat. III. Afferents from the lower brain stem. J Comp Neurol 1981;202:335–356. [PubMed: 7298902]

Phillips ML, Drevets WC, Rauch SL, Lane R. Neurobiology of emotion perception I: the neural basis of normal emotion perception. Biol Psychiatry 2003a;54:504–514. [PubMed: 12946879]

Phillips ML, Drevets WC, Rauch SL, Lane R. Neurobiology of emotion perception II: implications for major psychiatric disorders. Biol Psychiatry 2003b;54:515–528. [PubMed: 12946880]

Phillips RG, LeDoux JE. Differential contribution of amygdala and hippocampus to cued and contextual fear conditioning. Behav Neurosci 1992;106:274–285. [PubMed: 1590953]

Pitkanen A, Amaral DG. Distribution of calbindin-D28k immunoreactivity in the monkey temporal lobe: the amygdaloid complex. J Comp Neurol 1993;331:199–224. [PubMed: 7685361]

Pitkanen A, Amaral DG. Organization of the intrinsic connections of the monkey amygdaloid complex: projections originating in the lateral nucleus. J Comp Neurol 1998;398:431–458. [PubMed: 9714153]

Pitkanen A, Savander V, LeDoux JE. Organization of intraamygdaloid circuitries in the rat: an emerging framework for understanding functions of the amygdala. Trends Neurosci 1997;20:517–523. [PubMed: 9364666]

Porrino LJ, Crane AM, Goldman-Rakic PS. Direct and indirect pathways from the amygdala to the frontal lobe in rhesus monkeys. J Comp Neurol 1981;198:121–136. [PubMed: 6164704]

Price, JL.; Russchen, FT.; Amaral, DG. The limbic region. II. The amygdaloid complex. In: Hokfelt, BT.; Swanson, LW., editors. Handbook of chemical neuroanatomy. Elsevier; Amsterdam: 1987. p. 279-381.

Rosene DL, Roy NJ, Davis BJ. A cryoprotection method that facilitates cutting frozen sections of whole monkey brains for histological and histochemical processing without freezing artifact. J Histochem Cytochem 1986;34(10):1301–1315. [PubMed: 3745909]

Rosenkranz JA, Grace AA. Modulation of basolateral amygdala neuronal firing and afferent drive by dopamine receptor activation in vivo. J Neurosci 1999;19:11027–11039. [PubMed: 10594083]

Russchen FT. Amygdalopetal projections in the cat. II. Subcortical afferent connections. A study with retrograde tracing techniques. J Comp Neurol 1982;207:157–176. [PubMed: 7096644]

Russchen FT, Amaral DG, Price JL. The afferent input to the magnocellular division of the mediodorsal thalamic nucleus in the monkey, *Macaca fascicularis*. J Comp Neurol 1987;256:175–210. [PubMed: 3549796]

Sakamoto, N.; Pearson, J.; Shinoda, K.; Alheid, GF.; De Olmos, JS. The human basal forebrain. I. An overview. In: Bloom, FE.; Bjorkland, A.; Hokfelt, T., editors. Handbook of chemical neuroanatomy. Elsevier; Amsterdam: 1999. p. 1-56.

Schmued L, Kyriakidis K, Heimer L. In vivo anterograde and retrograde axonal transport of the fluorescent rhodamine-dextranamine, fluoro-ruby, within the CNS. Brain Res 1990;526:127–134. [PubMed: 1706635]

Sheline YI, Barch DM, Donnelly JM, Ollinger JM, Snyder AZ, Mintun MA. Increased amygdala response to masked emotional faces in depressed subjects resolves with antidepressant treatment: an fMRI study. Biol Psychiatry 2001;50:651–658. [PubMed: 11704071]

Siegle GJ, Steinhauer SR, Thase ME, Stenger VA, Carter CS. Can't shake that feeling: event-related fMRI assessment of sustained amygdala activity in response to emotional information in depressed individuals. Biol Psychiatry 2002;51:693–707. [PubMed: 11983183]

Swanson LW. The projections of the ventral tegmental area and adjacent regions: a combined fluorescent retrograde tracer and immunofluorescence study in the rat. Brain Res Bull 1982;9:321–353. [PubMed: 6816390]

Vercelli A, Repici M, Garbossa D, Grimaldi A. Recent techniques for tracing pathways in the central nervous system of developing and adult mammals. Brain Res Bull 2000;51:11–28. [PubMed: 10654576]

Wenzlaff RM, Wegner DM, Roper DW. Depression and mental control: the resurgence of unwanted negative thoughts. J Pers Soc Psychol 1988;55:882–892. [PubMed: 3216288]

Williams SM, Goldman-Rakic PS. Widespread origin of the primate mesofrontal dopamine system. Cereb Cortex 1998;8:321–345. [PubMed: 9651129]

Zahm DS, Jensen SL, Williams ES, Martin JR III. Direct comparison of projections from the central amygdaloid region and nucleus accumbens shell. Eur J Neurosci 1999;11:1119–1126. [PubMed: 10103108]

Zoli M, Torri C, Ferrari R, Jansson A, Zini I, Fuxe K, Agnati LF. The emergence of the volume transmission concept. Brain Res Brain Res Rev 1998;26:136–147. [PubMed: 9651506]

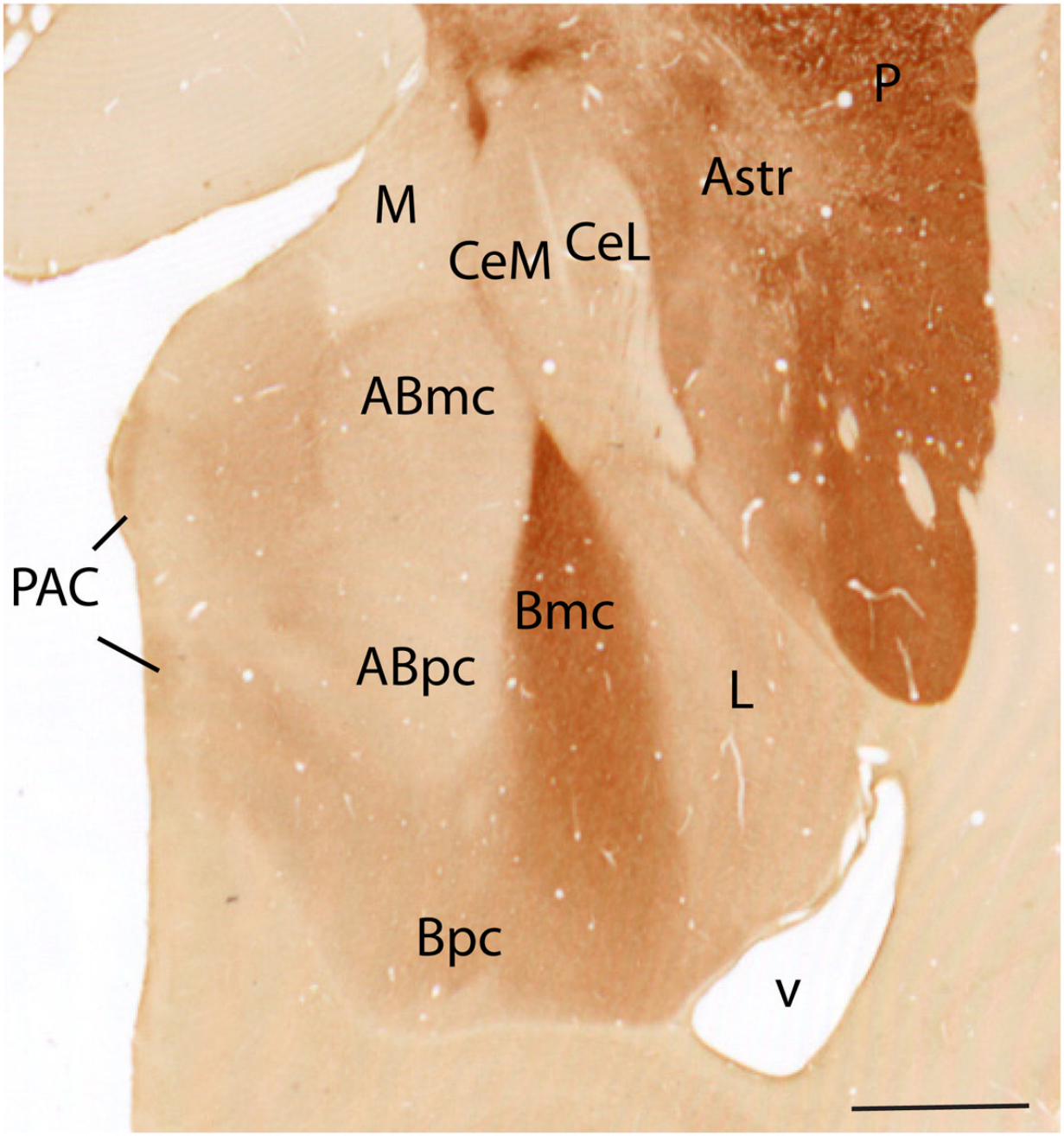

Fig. 1.

Acetylcholinesterase staining of *Macaca fascicularis* amygdala. Amygdala proper nuclei include Abmc, accessory basal, magnocellular; Abpc, accessory basal, parvicellular; ABs, accessory basal, sulcus; Bi, basal, intermediate; Bmc, basal, magnocellular; Bpc, basal, parvicellular; L, lateral. Central extended amygdala nuclei at this level include CeM, central nucleus, medial subdivision; CeL, central nucleus, lateral core subdivision; Astr, amygdalostriatal area; M, medial nucleus; CoP, cortical nucleus, posterior; P, putamen, PAC, periamygdaloid cortex; v, ventricle. Scale bar=1 mm. For interpretation of the references to color in this figure legend, the reader is referred to the Web version of this article.

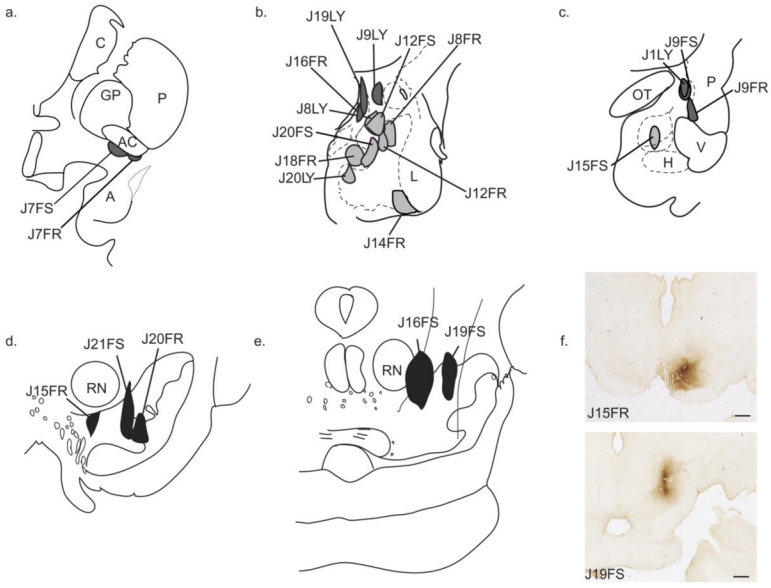

Fig. 2.

Schematic of all injection sites. Retrograde injections (a–c): (a) Injection sites in the IPAC (J7FR, J7FS). (b) Injection sites in the "amygdala proper" are colored light gray: Bmc (J8FR, J12FR); ABmc (J8LY, J12FS); ABpc (J18FR, J20FS); Bpc (J14FR, J20LY). Injections sites in the "extended amygdala" are colored dark gray: CeM (J9LY); MeN (J16FR, J19LY). (c) Injection sites in the caudal "amygdala proper": Bpc (J15FS). Injection sites in caudal extended amygdala: CeLcn (J1LY, J9FS); Amygdalostriatal area (J9FR). Anterograde injections (d–f): (d) Injection sites in the A9-SNpc: medial A9-SNpc (J15FR); mediolateral A9-dt and A9-vt (J21FS); medial A9-vt (J20FR). (e) Injections sites in the A8-RRF: rostromedial A8-RRF (J19FS); caudomedial A8-RRF (J16FS). (f) Photomicrographs of injection sites: J15FR—medial A9-SNpc (top); J19FS—rostromedial A8-RRF (bottom). FR, Fluoro Ruby; FS, Fluorescein; LY, Lucifer Yellow. Scale bar=1 mm. For interpretation of the references to color in this figure legend, the reader is referred to the Web version of this article.

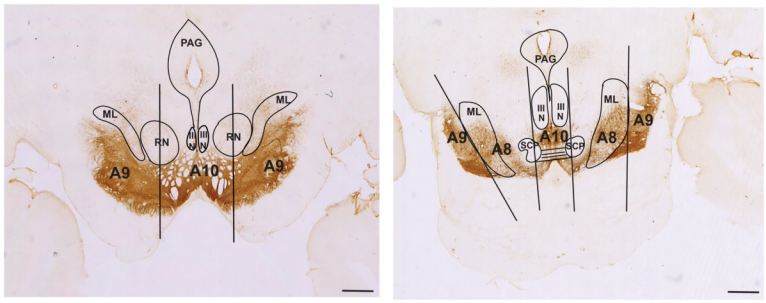

Fig. 3.

Boundaries of midbrain dopaminergic groups. Coronal sections stained for TH-immunoreactivity. At more rostral levels (left), A10 was bound laterally by a line bisecting the red nucleus (RN) in half. A9 was bound medially by this line, and dorsolaterally by the medial lemniscus (ML). Caudally (right), A10 resided medial to the lateral border of cranial nerve III (III N). A8 was defined between the lateral edge of cranial nerve III and the lateral edge of the ML. Extensions of A9 were lateral to the lateral edge of ML. Scale bar=1 mm. For interpretation of the references to color in this figure legend, the reader is referred to the Web version of this article.

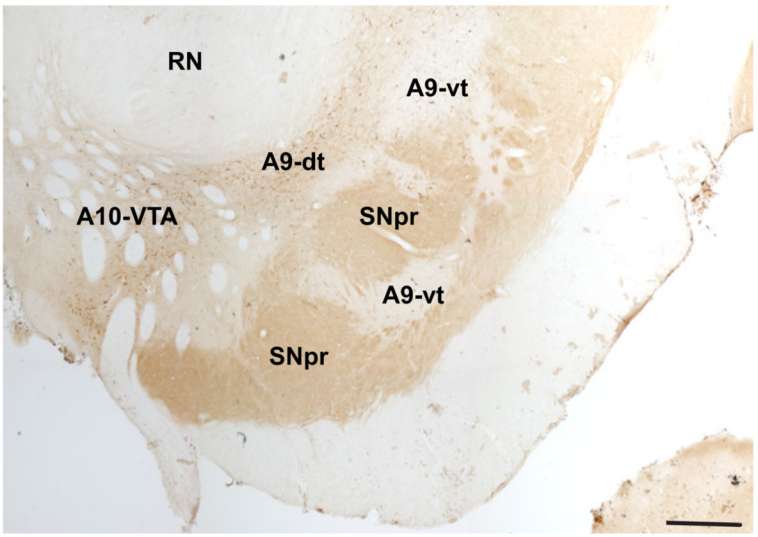

Fig. 4.

Subdivisions of the A9 group. Coronal section stained for calbindin-28k (CABP) immunoreactivity. A9-dt (dorsal tier) contains CABP-positive soma; A9-vt (ventral tier) is CABP-negative; SNpr (substantia nigra, pars reticulata) stains for CABP-positive fibers. Note, A10-VTA stains for CABP-positive soma and is also considered part of the dorsal tier, but is separate from A9-dt. Scale bar=1 mm. For interpretation of the references to color in this figure legend, the reader is referred to the Web version of this article.

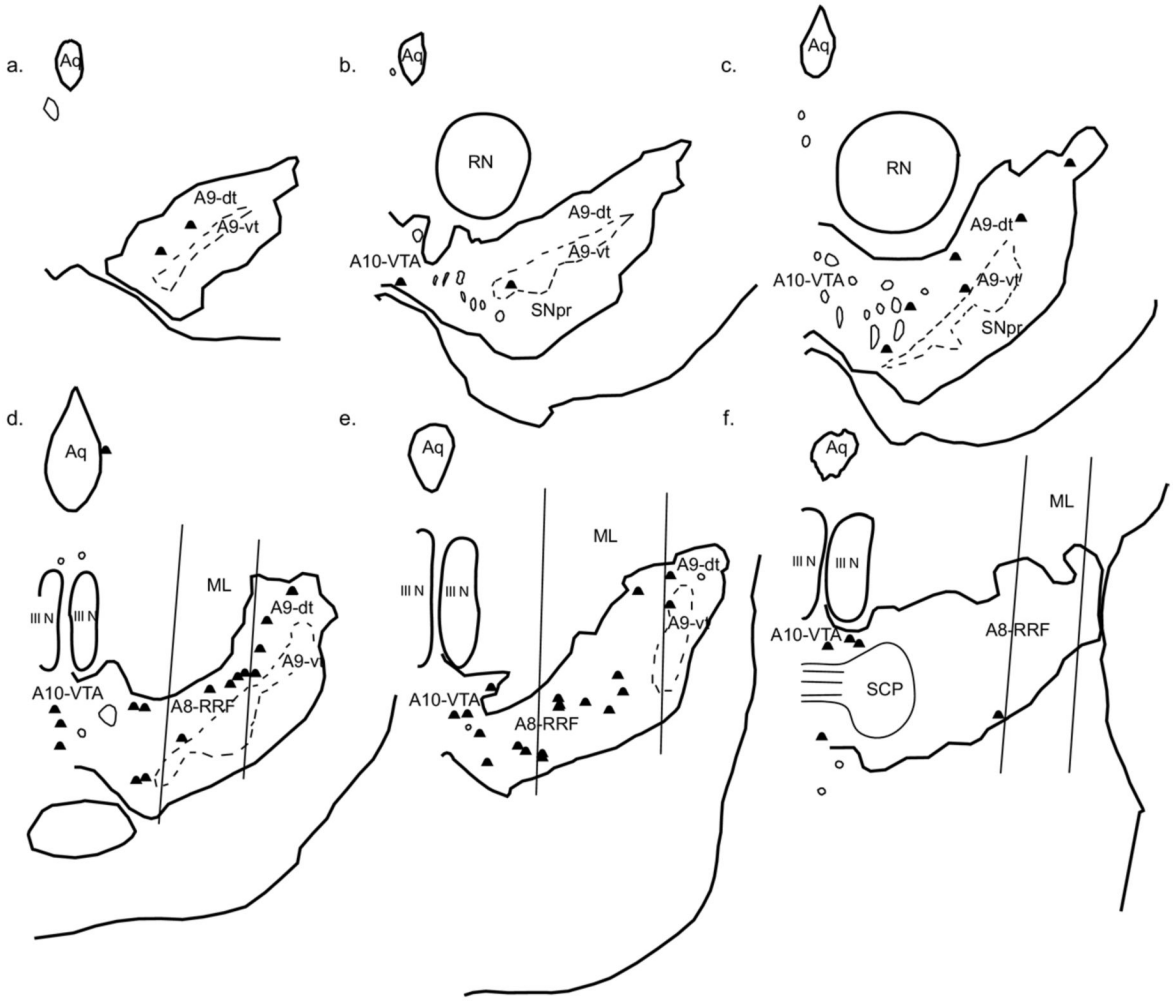

Fig. 5.

Double-labeled cells resulting from an injection in the basal, magnocellular (Bmc, case J12FR). One dot represents one double-labeled cell. (a–f) depict sections from rostral to caudal.

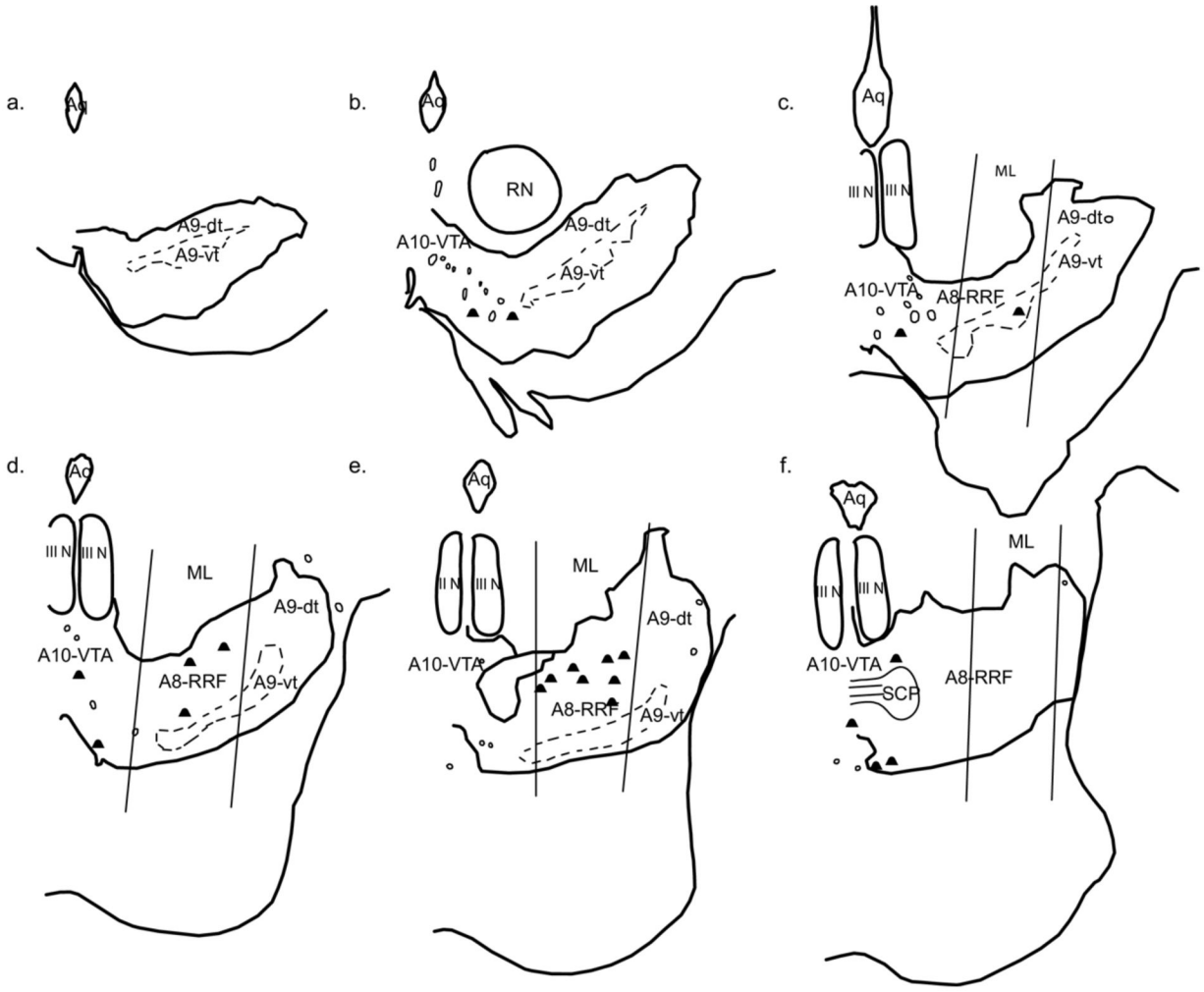

Fig. 6.

Double-labeled cells resulting from an injection in the basal, parvicellular nucleus (Bpc, case J14FR). Each dot represents one double-labeled cell. (a–f) depict sections from rostral to caudal.

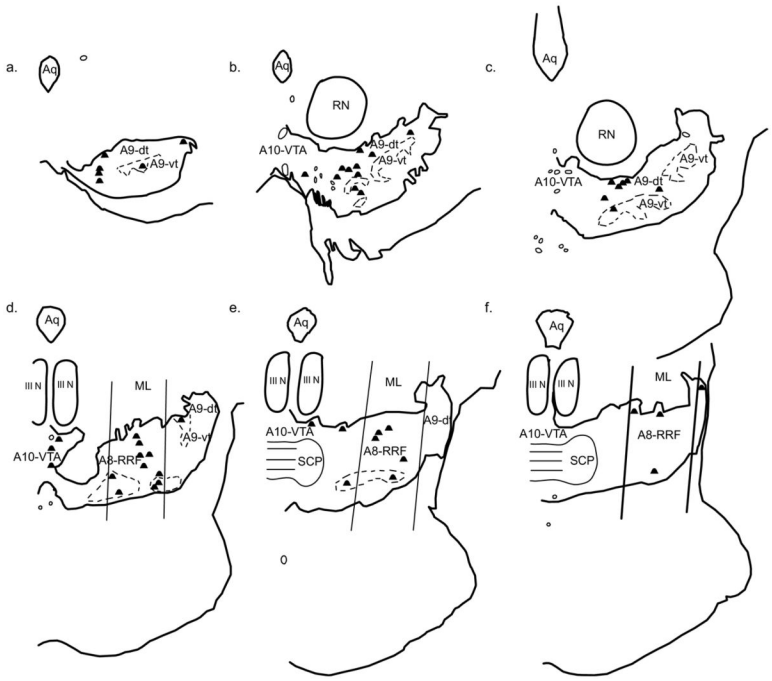

Fig. 7.

Double-labeled cells resulting from an injection in the medial nucleus (MeN, case J19LY). Each dot represents one double-labeled cell. (a–f) depict sections from rostral to caudal.

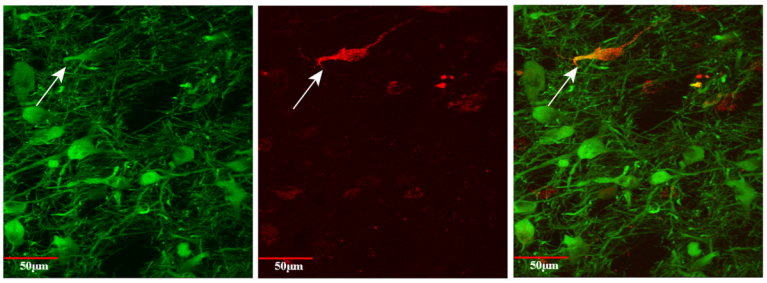

Fig. 8.

Double-labeled cell viewed with confocal microscopy at 40×. TH is labeled in green (left) (488 nm, Alexafluor). Tracer is labeled in red (middle) (596 nm, Texas Red, Genway). Merged picture showing double-labeling is shown at right. Taken from the A8-RRF following injection into the MeN (J16FR). Note the large size, and prominent proximal dendrites of TH-containing cells. For interpretation of the references to color in this figure legend, the reader is referred to the Web version of this article.

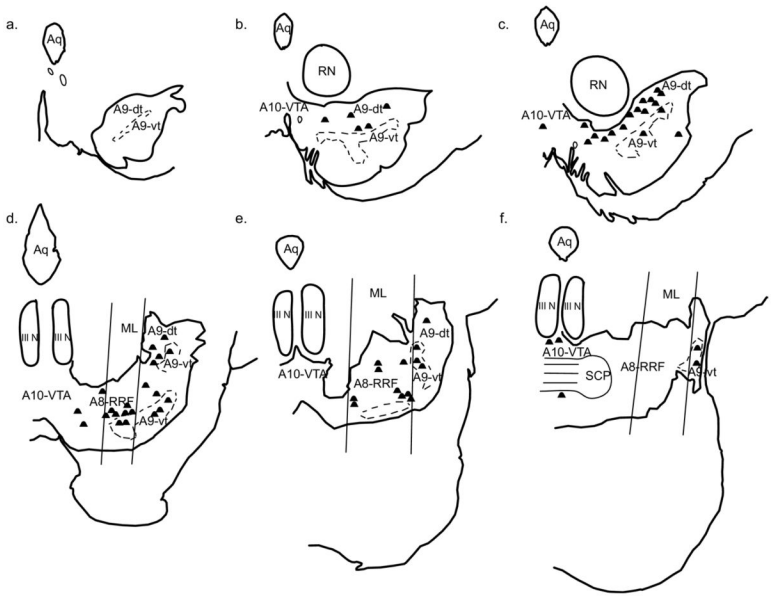

Fig. 9.

Double-labeled cells resulting from an injection in the central nucleus, medial division (CeM, case J9LY). Each dot represents one double-labeled cell. (a–f) depict sections from rostral to caudal.

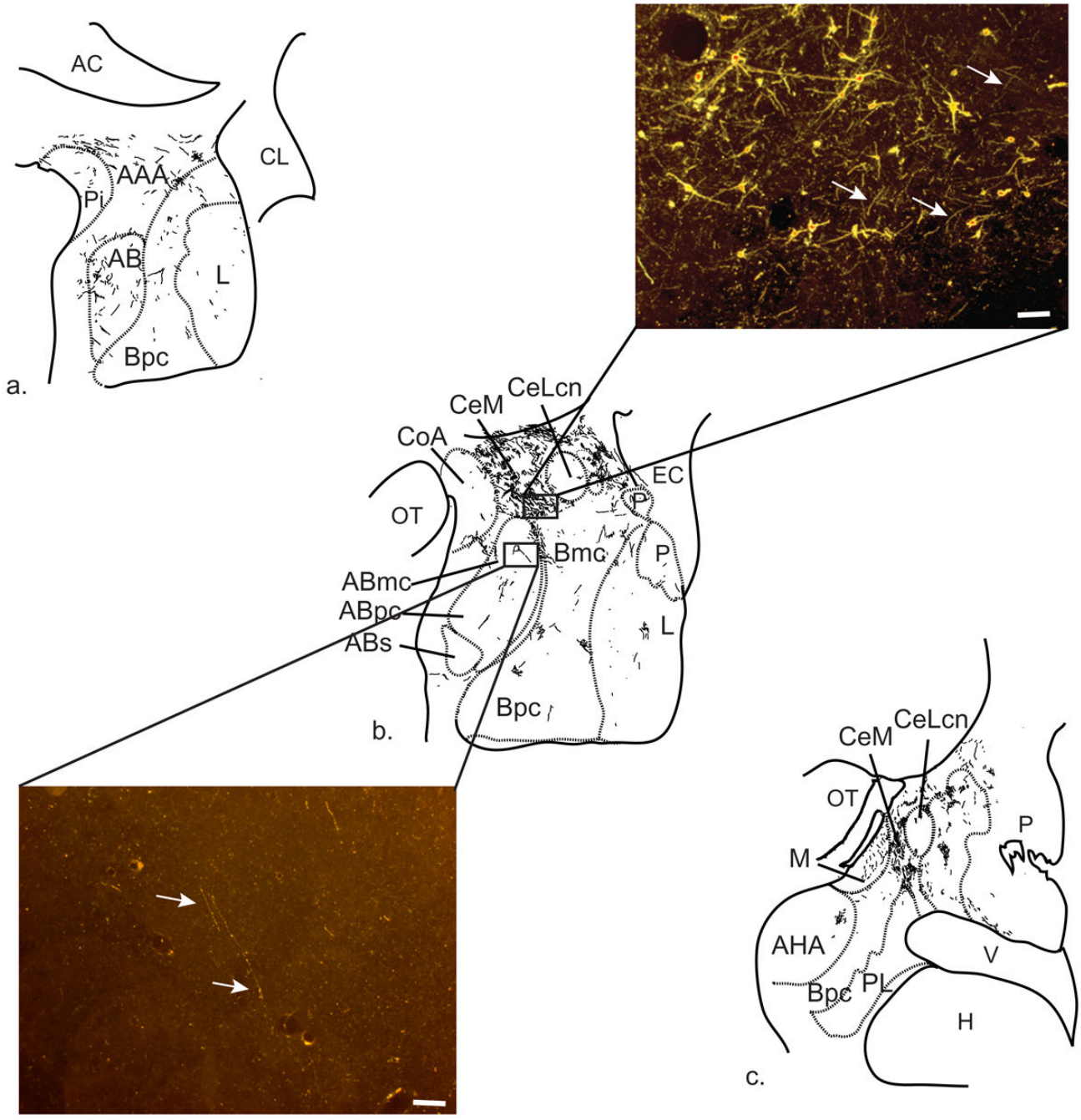

Fig. 10.

Distribution of anterograde-labeled fibers in amygdala following A8-RRF injection (J19FS). (a) Rostral portion of primate amygdala. (b) Amygdala at mid-rostrocaudal level. Note the greater density of fiber labeling around the CeM, with less dense labeling in the amygdala proper. The CeLcn is nearly devoid of anterograde fiber labeling. Associated photomicrographs of CeM (top)—note presence of cell bodies indicating projections back to the midbrain, and ABmc (bottom) stained for tracer and viewed under 10× dark-field microscopy. Scale bar=50 μm. (c) Caudal portion of the amygdala. The CeM continues to receive a dense projection from the A8-RRF at this level. For interpretation of the references to color in this figure legend, the reader is referred to the Web version of this article.

Fig. 11.

Composites of double-labeled cells following all injection sites. Most labeled cells lie along the A9-dt (left) and A8-RRF (right). A modest amount of cells are present in the A10-VTA. Gray dots indicate double-labeled cells resulting from all injections into the amgdala proper. Black dots indicate double-labeled cells resulting from all injections into the extended amygdala.

Table 1

List of injection sites with corresponding case numbers

Area of injection	Case number(s)	Tracer direction
Amygdala proper		
Basal—magnocellular	J8FR, J12FR	Retrograde
Basal—parvicellular	J14FR, J15FS, J20LY	Retrograde
Accessory basal—magnocellular	J8LY, J12 FS	Retrograde
Accessory basal—parvicellular	J18FR, J20FS	Retrograde
Extended amygdala		
Central nucleus—medial	J9LY	Retrograde
Central nucleus—lateral	J1LY, J9FS	Retrograde
Medial nucleus	J16FR, J19LY	Retrograde
Amygdalostriatal	J9FR	Retrograde
IPAC	J7FR, J7FS	Retrograde
Dopaminergic groups		
A9-substantia nigra—dorsal tier	J15FR, J21FS	Anterograde
A9-substantia nigra—ventral tier	J20FR	Anterograde
A8-retrorubral field	J16FS, J19FS	Anterograde

All tracers are bidirectional and “tracer direction” indicates the direction used for analysis of our study.

LY, lucifer yellow; FR, fluoro ruby; FS, fluoroscein.

Table 2

Relative input from TH-positive cell groups to amygdalar nuclei

Area of injection	A10-VTA	A9-SN-dt	A9-SN-vt	A8-RRF
Extended amygdala				
Central nucleus—medial	++	++++	++	+++
Amygdalostriatal	+	++++	+++	+
IPAC	++	++	−	++
Medial nucleus	++	++	+	+++
Amygdala proper				
Basal—magnocellular	+++	++	−	++
Accessory basal—magnocellular	++	++	+	++
Basal—parvicellular	+	+	−	++
Accessory basal—parvicellular	+	+	−	+

−, no labeled cells; +, 1−7 labeled cells; ++, 8–14 labeled cells; +++, 15–21 labeled cells; ++++, 22–28 labeled cells. CeLcn not included.